Nano Research
2020, 13(9): 2365–2370
ISSN 1998-0124 CN 11-5974/O4
https://doi.org/10.1007/s12274-020-2856-z

Research Article

Highly active N-doped carbon encapsulated Pd-Fe intermetallic nanoparticles for the oxygen reduction reaction

Yezhou Hu[1], Yun Lu[1], Xueru Zhao[2], Tao Shen[1], Tonghui Zhao[1], Mingxing Gong[1], Ke Chen[1], Chenglong Lai[1], Jian Zhang[1], Huolin L. Xin[3], and Deli Wang[1] (✉)

[1] *Key laboratory of Material Chemistry for Energy Conversion and Storage (Huazhong University of Science and Technology), Ministry of Education, Hubei Key Laboratory of Material Chemistry and Service Failure, School of Chemistry and Chemical Engineering, Huazhong University of Science and Technology, Wuhan 430074, China*

[2] *Institute of New-Energy Materials, Key Laboratory of Advanced Ceramics and Machining Technology of Ministry of Education, School of Materials Science and Engineering, Tianjin University, Tianjin 300072, China*

[3] *Department of Physics and Astronomy, University of California, Irvine, Irvine, CA 92697, USA*

Received: 9 April 2020 / **Revised:** 5 May 2020 / **Accepted:** 6 May 2020

ABSTRACT

Developing highly efficient non-Pt catalysts for fuel cells and metal-air batteries is highly desirable but still challenging due to the sluggish oxygen reduction reaction (ORR). Herein, a facile and efficient strategy is demonstrated to prepare N-doped carbon encapsulated ordered Pd-Fe intermetallic (O-Pd-Fe@NC/C) nanoparticles via a one-step thermal annealing method. The obtained O-Pd-Fe@NC/C nanoparticles show enhanced ORR activity, durability and anti-poisoning capacity in both acid and alkaline medium. When O-Pd-Fe@NC/C serving as cathode catalyst for Zn-air battery, it exhibits higher voltage platform and superior cycling performance with respect to the Zn-air battery based on the mixture of Pt/C and Ir/C catalysts. The enhanced electrocatalytic performance can be ascribed to the formation of face-centered tetragonal (fct) Pd-Fe nanoparticles, the protective action of the N-doped carbon layer and the interface confinement effect between them. The *in situ* formed N-doped carbon shell not only restrains the Pd-Fe ordered intermetallics from aggregating effectively during the thermal annealing process, but also provides a strong anchoring effect to avoid the detachment of Pd-Fe nanoparticles from the carbon support during the potential cycling. This facile carbon encapsulation strategy may also be extended to the preparation of a wide variety of N-doped carbon encapsulated intermetallic compounds for fuel cell application.

KEYWORDS

palladium, carbon encapsulation strategy, ordered intermetallic nanoparticles, oxygen reduction reaction (ORR), Zn-air battery

1 Introduction

Fuel cells have been considered as one of the promising energy conversion devices due to its environmental-friendly merits, high power density, and high efficiency, etc. [1, 2]. While, the overall performance of fuel cells is limited due to the sluggish oxygen reduction reaction (ORR), which seriously restricts the development [3, 4]. Currently, Pt-based nanomaterials are the most commonly used ORR electrocatalysts in fuel cells. Whereas, the large-scale application of Pt in fuel cells is limited by its prohibitive costs, relatively low abundance and poor poison tolerance performance [5–7]. Therefore, exploring alternative non-Pt catalysts with higher electrocatalytic activity, superior durability, relative abundance, and unique anti-poisoning property is of great significance for the commercialization of fuel cells.

Pd-based electrocatalysts are regarded as viable alternatives to Pt for ORR in both acidic and alkaline electrolyte due to its relative abundance and Pt-like properties [8, 9]. Inspired by this, considerable efforts have been made to design Pd-based catalysts with desirable size [10], compositions [11, 12], and shape [13, 14]. Among them, much attention is on the disordered Pd-based alloy. However, such disordered Pd-based alloy catalysts still suffer from limited electrocatalytic performance and low stability as the randomly distributed transition metal is rapidly leached in the acid environment [15, 16]. In these regards, exploring structurally ordered Pd-based catalysts with definite composition and structure is of great significance for the improvement of electrocatalytic ORR performance. In our previous work, the ordered intermetallic tetragonal phase Pd-Fe nanoparticles exhibit improved electrocatalytic activity and stability compared to face-centered cubic (fcc) one [17].

But, the stability of Pd-based catalysts should be further improved as inevitable metal leaching, aggregation, and detachment of nanoparticles from the support during the fuel cell operation greatly affect the electrocatalytic performance. Furthermore, the high-temperature post-annealing treatment is usually required to achieve this structure transformation, inevitably leading to the aggregation of nanoparticles, and thus decreasing the number density of active sites [1, 18, 19]. Recently, numerous efforts have been made to address these problems by confining nanoparticles into protective coating such as graphitic hollow spheres [20], physical barriers [21], inorganic barriers [22], etc. However, the presence of these

Address correspondence to wangdl81125@hust.edu.cn

protective layers usually blocks the active sites and some of them even isolates the active sites from electrolyte, thus decreasing the electrocatalytic performance. In order to expose the active sites, additional steps are usually required, which is time-consuming and in turn hinders the development of fuel cells.

Herein, we demonstrate a facile one-pot strategy to prepare N-doped carbon encapsulated ordered intermetallic Pd-Fe (O-Pd-Fe@NC/C, 'O' represents the alloy is with ordered crystal structure) nanoparticles. The *in situ* formed N-doped carbon shell can not only act as a protective layer to prevent the nanoparticles aggregation or detachment from the carbon support, but also significantly affect the inner Pd-Fe ordered intermetallics to synergistically improve the ORR activity during the electrocatalysis. As a result, the O-Pd-Fe@NC/C nanoparticles exhibit superior catalytic activity and excellent stability for ORR.

2 Results and discussion

2.1 Synthesis and characterization of N-doped carbon encapsulated Pd-Fe intermetallic

The synthesis procedure of O-Pd-Fe@NC/C is illustrated in Scheme 1. The Pd^{2+}/Fe^{2+}/ dicyandiamide (DCDA) functionalized carbon black was first prepared by the impregnation method. The obtained powder was then heated at 800 °C for 2 h. DCDA serves as the both nitrogen and carbon source for the formation of N-doped carbon shell. During this heating process, Pd^{2+} and Fe^{2+} were gradually reduced to form Pd-Fe alloy, and DCDA might be converted to melamine first and then turned into the layered C_3N_4 at the low temperature [23]. With the temperature increasing, such layered C_3N_4 intermediates would be further decomposed, and simultaneously catalyzed by inner Pd-Fe alloy to form a thinner N-doped carbon layer [24]. Meanwhile, the ordered intermetallic Pd-Fe nanoparticles can also be achieved and imbedded into the carbon layer.

Powder X-ray diffraction (XRD) patterns are shown in Fig. 1(a), a broad peak located at ~ 25° can be observed for the catalysts, which is ascribed to the existence of carbon support. Typically, the O-Pd-Fe@NC/C shows the superlattice reflection peaks such as (001), (201), (112), (202), (003) and (310) planes compared with D-Pd-Fe/C ('D' represents that the PdFe alloy is with disordered atom arrangement) and Pd/C, indicating that the face-centered tetragonal (fct) phase exists in the Pd-Fe nanoparticles. The corresponding fast Fourier transtorm (FFT) pattern in Fig S1(a) in the Electronic Supplementary Material (ESM) also confirms the intermetallic structure of O-Pd-Fe@NC/C. The high-resolution transmission electron microscopy (HR-TEM) was used to characterize the morphology of the catalyst (Figs. 1(b) and 1(c), and Fig. S1(b) in the ESM). The TEM images in Figs. 1(b) and 1(c) show carbon layers with thickness of ~ 2.6 nm are *in situ* formed on O-Pd-Fe nanoparticles, which is ascribed to the evolution of CN_x species released from DCDA along with the catalytic action of the inner Pd-Fe [22]. In Fig. 1(d), some pores can be visualized from the carbon shell.

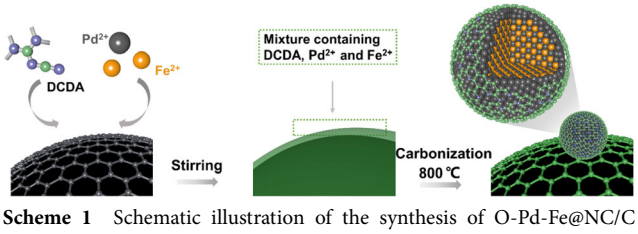

Scheme 1 Schematic illustration of the synthesis of O-Pd-Fe@NC/C catalysts via one-pot annealing method.

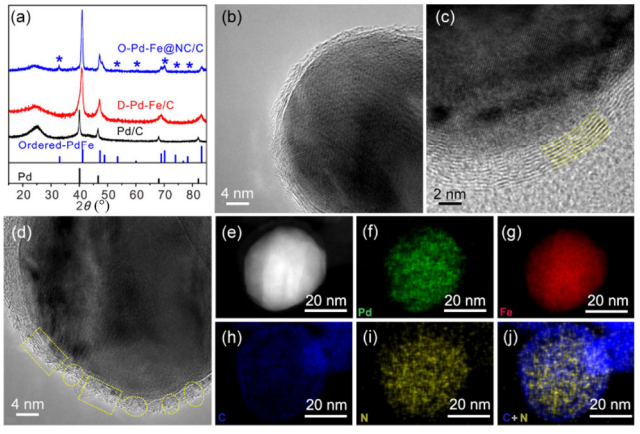

Figure 1 (a) XRD patterns of Pd/C, disordered Pd-Fe (D-Pd-Fe/C) and N-doped carbon encapsulated Pd-Fe ordered intermetallics (O-Pd-Fe@NC/C), the asterisk indicates the superlattice peaks of Pd-Fe ordered intermetallics. (b)–(d) HR-TEM images of O-Pd-Fe@NC/C nanoparticles. (e)–(j) High-angle annular dark-field (HAADF)-STEM patterns and EDS elemental mappings of Pd, Fe, C, N and the composite of C and N.

This could be explained by the CN_x gases released from the C_3N_4 during the thermal treatment of DCDA [25]. To characterize the elemental distribution of encapsulation-structure, scanning transmission electron microscopy (STEM) equipped with energy dispersive X-ray spectroscopy (EDS) was performed (Figs. 1(e)–1(j)). It can be clearly seen that the EDS elemental maps of Pd and Fe are in accordance with the STEM images, indicating the highly ordered structure of O-Pd-Fe@NC/C nanoparticles. The EDS elemental maps of C, N and the composites of C and N confirm that the Pd-Fe ordered intermetallics are well encapsulated in the carbon layer and N element is mainly distributed in the carbon layer.

Besides, X-ray photoelectron spectroscopy (XPS) was used to reveal the element compositions and the possible interaction between Pd-Fe ordered intermetallic nanoparticles and N-doped carbon layer. As seen from Fig. 2(a), the XPS signal of N 1s can only be observed in O-Pd-Fe@NC/C nanoparticles. The N 1s spectrum of O-Pd-Fe@NC/C is deconvoluted into three characteristic peaks (Fig. 2(b)). The peaks located at 398.4, 400.7 and 404.6 eV can be attributed to pyridinic N, graphitic N and oxidized N, respectively [26]. Generally, graphitic N and pyridinic N have been reported to be favorable for the ORR [27]. In Fig. 2(c), the fitted C 1s results also confirm the

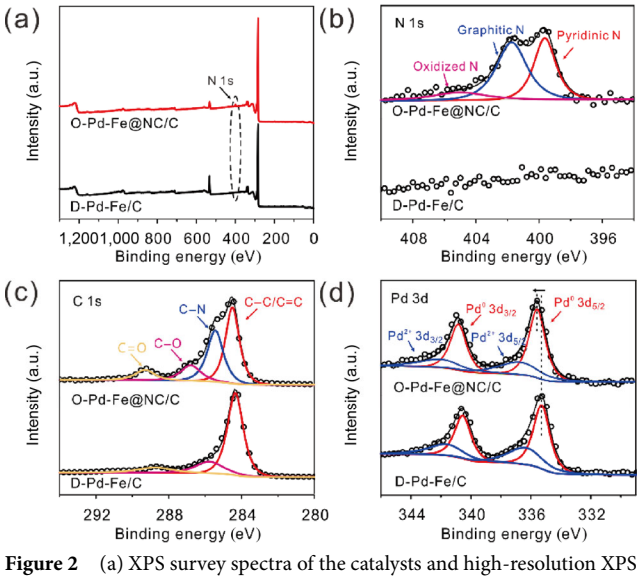

Figure 2 (a) XPS survey spectra of the catalysts and high-resolution XPS spectra showing (b) N 1s, (c) C 1s, and (d) Pd 3d in full scan.

formation of N dopants in the O-Pd-Fe@NC/C. To further reveal the possible interface confinement effect between Pd-Fe ordered intermetallic nanoparticles and the N-doped carbon layer. In Fig. S2(a) in the ESM, the high resolution spectrum of Fe 2p shows three different couples of peaks, which can be assigned to Fe^0 (707.1 eV), Fe^{2+} (710.7 eV) and Fe^{3+} (714.6 eV), illustrating the partial oxidation of Fe due to the exposure under the ambient air. Figure S2(b) in the ESM shows the high spectrum of O 1s for O-Pd-Fe@NC/C. The high-resolution XPS signal of Pd 3d for O-Pd-Fe@NC/C and Pd-Fe/C are analyzed. As shown in Fig. 2(d), the binding energies for Pd 3d peaks in O-Pd-Fe@NC/C exhibit shifts of 0.45 eV toward higher value compared to that of D-Pd-Fe/C. The shift could be explained by the possible electronic interaction that happens on the interference of N-doped carbon shell and Pd-Fe ordered core, which remarkably affects the electronic structure of Pd, and thus leading to the enhanced electrocatalytic performance [28]. Furthermore, previous studies have proved that the N doping in carbon matrix influences not only the properties of carbon but also the metal nearby. Arrigo and co-workers [29] have proposed that the hybridization between π-orbitals of N and d-orbitals of metal may be involved in the interaction between the N and metal, thus prompting the electrical conductivity and offering strong support-metal interaction (SMI). To further reveal the vital role N-doped carbon played in the thermal stability of O-Pd-Fe@NC/C, the thermal gravimetric and derivative thermogravimetry (TG/DTG) analyses are conducted (Fig. S3 in the ESM). The significant weight loss results from the decomposition of carbon black. It is clear that O-Pd-Fe@NC/C nanoparticles show higher decomposition temperature, indicating the higher degree of graphitization and higher thermal stability of the carbon shell, which could be attributed to the high-temperature treatment and the incorporation of N element into carbon layer [30].

2.2 Electrochemical performance of the N-doped carbon encapsulated Pd-Fe intermetallic

The electrocatalytic ORR performance of the catalysts was evaluated using rotating disk electrode (RDE) technique. In Fig. 3(a), the ORR polarization curves demonstrate that the O-Pd-Fe@NC/C exhibits the highest half-wave potentials among the catalysts. This is well in accordance with their ORR peak position observed from cyclic voltammetry (CV) curves (Fig. 3(b)). The potential of ORR cathodic peaks shifts to higher position for O-Pd-Fe@NC/C, indicating the lower oxygen adsorption energy [31, 32]. In Figs. 3(c) and 3(d), the mass activities (MA) and specific activities (SA) of the catalysts before and after accelerating degradation tests (ADT) are further compared, and Fig. S4 in the ESM shows the corresponding CV and LSV curves. The MA of O-Pd-Fe@NC/C is 0.32 $A \cdot mg_{Pd}^{-1}$, which is more than double that of D-Pd-Fe/C (0.14 $A \cdot mg_{Pd}^{-1}$), and even exceeds that of Pt/C (0.25 $A \cdot mg_{Pt}^{-1}$). The SA of O-Pd-Fe@NC/C (0.78 $mA \cdot cm^{-2}$) is also enhanced, more than twice of that of Pt/C (0.33 $mA \cdot cm^{-2}$). To confirm the positive contribution made by N-doped carbon to the enhancement of ORR performance, the N-doped carbon supported on carbon black (NC/C) was prepared and its ORR activity was tested under the same condition (Fig. S5 in the ESM). The NC/C shows slightly enhanced ORR activity compared with carbon black, indicating that the N-doped carbon may not be the direct influencing factor for the enhanced ORR performance. Therefore, the interface confinement effect between N-doped carbon shell and Pd-Fe ordered intermetallic structure may play a vital role in the enhanced electrocatalytic performance of O-Pd-Fe@NC/C. In order to investigate the ORR kinetic

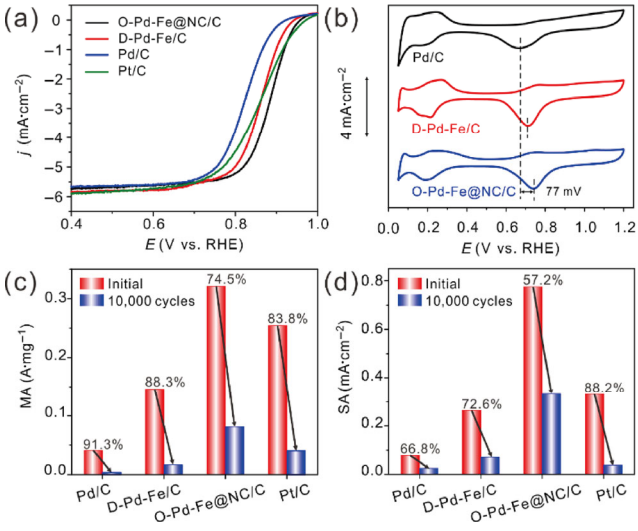

Figure 3 (a) LSV curves and (b) CV curves of the catalysts recorded in 0.1 M $HClO_4$. (c) Comparison of MA and (d) SA calculated at 0.85 V (vs. RHE) before and after ADT.

characteristic of O-Pd-Fe@NC/C, the ORR polarization curves were recorded with different rotation rates (Fig. S6 in the ESM). Corresponding to the fitted Koutecky-Levich plots of the catalysts, good linearity and parallelism can be observed. The slops of these curves are nearly constant at 0.7, 0.75 and 0.8 V, suggesting that the ORR process follows the first-order reaction kinetics toward the concentration of dissolved O_2 [33]. Besides, the average electron transfer number of O-Pd-Fe@NC/C is ~ 4.0, basically agrees with the theoretical value.

Long-term stability is another important factor for the electrocatalysts. Among them (Fig. 3(d)), O-Pd-Fe@NC/C still shows the highest MA and SA with the smallest attenuation rate after long-term stability test, indicating that O-Pd-Fe@NC/C shows better durability than the others. After ADT, XPS was carried out to study the N and Pd element on O-Pd-Fe@NC/C. Figure S7(a) in the ESM shows that three peaks are corresponding to the different types of N dopant in O-Pd-Fe@NC/C. Deserved to be mentioned, the peak intensity corresponding to pyridinic N shows a significant decrease, from 38% to 16%, this can be attributed to the instability of pyridinic N during potential cycling in acid solution [30]. Note that the Pd 3d spectrum has nearly no change even after long-term stability test (Fig. S7(b) in the ESM). According to morphology characterization after durability test shown in Fig. S8 in the ESM, such core-shell still remains intact, which is also confirmed by the EDX mapping shown in Fig. S9 in the ESM. In addition, the chemical compositions of the surface of O-Pd-Fe@NC/C after 10,000 cycles are also supplied as can be seen in Table. S1 in the ESM. Thus we conclude that the N-doped carbon shell could effectively prevent the oxidation of Pd due to the strong interaction between them.

Despite the superior electrocatalytic activity and durability, the collapse of fuel cell performance due to the strongly adsorbed species such as CO and SO_x, is still a serious issue. Therefore, the anti-poisoning effect of O-Pd-Fe@NC/C on these species was evaluated by CO stripping technology and LSV technology in the presence of SO_3^{2-}. Figure S10(a) in the ESM shows the representative CO-stripping curves for the catalysts. The CO stripping potentials show negative shift of 46 mV for D-Pd-Fe/C and 90 mV for O-Pd-Fe@NC/C, indicating the enhanced CO anti-poisoning capacity with respect to Pd/C [34]. Also, the ORR activities of O-Pd-Fe@NC/C catalysts in the presence of SO_3^{2-} were tested to assess the anti-poisoning effect on SO_3^{2-} (Fig. S10(b) in the ESM). Clearly,

Pd/C is highly sensitive to SO_3^{2-}, with a negative shift of half-wave potential of 208 mV, whereas O-Pd-Fe@NC/C exhibits the weakest decay of half-wave potential 14 mV. The results indicate that the O-Pd-Fe@NC/C has superior anti-poisoning capacity, which may be ascribed to the incorporation of Fe into Pd and the carbon encapsulation, thus weakening the adsorption of poisoning species [35].

Moreover, the electrocatalytic ORR activity and stability of O-Pd-Fe@NC/C in basic medium were also evaluated. As shown in Fig. 4(a), the O-Pd-Fe@NC/C shows the highest performance (~ 0.91 V) among them. Their CV curves in Fig. 4(b) also conform to the same trend of activities for the catalysts. This enhancement could be ascribed to the weakened oxygen adsorption energy caused by the interface confinement effect that happens on the interference of N-doped carbon shell and Pd-Fe ordered intermetallics. We also compared the ORR performance of as-prepared O-Pd-Fe@NC/C with the results of previously reported publication (Table S2 in the ESM).

Similarly, the linear sweep voltammetry (LSV) curves O-Pd-Fe@NC/C were recorded with different rotation rates (Fig. S11 in the ESM). The average electron transfer number in the ORR is calculated to be ~ 3.9 based on the result of K-L plots obtained at 0.7, 0.75 and 0.8 V in the case of O-Pd-Fe@NC/C, approaching the value of Pt/C (~ 4.0), also demonstrating that oxygen molecules are completely reduced for these catalysts. Also, the good linearity and parallelism demonstrate that its ORR kinetics is the first-order reaction with O_2, which accords with the theoretical value.

The durability test of O-Pd-Fe@NC/C in alkaline solution was also performed. As revealed in Fig. 4(c) and Fig. S13 in the ESM, after potential cycling between 0.6 and 1.0 V in O_2-saturated $HClO_4$ for 30,000 cycles, the decay of half-wave potential of O-Pd-Fe@NC/C is only 2 mV, while the value of Pt/C is up to 63 mV. Further, the chronoamperometric analysis results (Fig. S12 in the ESM) also show that the percentage retention of the catalytic current for O-Pd-Fe@NC/C (93%), while a relatively lower current retention is observed for Pt/C (64%). These results indicate that O-Pd-Fe@NC/C possesses excellent stability in 0.1 M KOH. Furthermore, the methanol crossover effect and adsorption of methanol moieties on the surface of the catalyst may generate a mixed potential and thus influencing the performance [36–39]. Therefore, the methanol tolerance of O-Pd-Fe@NC/C was studied by adding methanol in the chronoamperometric test. Figure 4(d) shows the chronoamperometric responses of O-Pd-Fe@NC/C and Pt/C catalysts in the presence of 0.5 M methanol. A significant methanol oxidation current can be observed when injecting methanol at 100 s for Pt/C, while a relatively lower methanol oxidation current peak appears in the case of O-Pd-Fe@NC/C, indicating the great methanol tolerance of O-Pd-Fe@NC/C for ORR. These results demonstrate that the as-synthesized O-Pd-Fe@NC/C has the advantages of selectivity towards ORR and methanol tolerance.

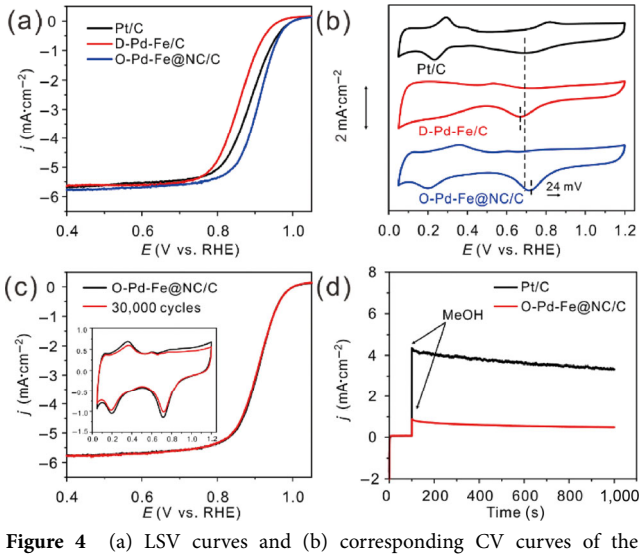

Figure 4 (a) LSV curves and (b) corresponding CV curves of the catalysts. (c) LSV curves for O-Pd-Fe@NC/C before and after durability test, insert shows the corresponding CV curves. (d) The chronoamperometric responses for the catalysts in the presence of 0.5 M methanol.

Based on above-mentioned results and analyse, we ascribe the enhanced ORR performance of O-Pd-Fe@NC/C to the following points. (1) The compressive lattice strain derived from the incorporation of Fe into Pd and ordered structure of O-Pd-Fe@NC/C, which may be responsible for the lowered oxygen adsorption energy. (2) The interface confinement effect between the Pd-Fe ordered intermetallic nanoparticles and N-doped carbon shell. (3) The strong anchoring effect of N-doped carbon shell and thus forming strong SMI effect.

2.3 Zn-air battery test

Given the superior ORR property O-Pd-Fe@NC/C presented above, a homemade Zn–air battery was established with O-Pd-Fe@NC/C acting as the cathode catalyst and polished Zn foil serving as the anode (Fig. 5(a)). In Fig. 5(b), we can see that the assembled Zn-air battery demonstrates a high open circle potential of 1.43 V for a long duration. As revealed in Fig. 5(c), the O-Pd-Fe@NC/C-based Zn-air battery exhibits a high peak power density of 169 $mW \cdot cm^{-2}$. In Fig. 5(d), when normalized the mass of consumed Zn foil, the specific capacity of O-Pd-Fe@NC/C reaches as high as 779 $mAh \cdot g^{-1}$, the value of which is also higher than that of Pt/C (725 $mAh \cdot g^{-1}$). The O-Pd-Fe@NC/C-based battery also exhibits excellent rate capability and stable voltage plateaus at different discharge current density (Fig. 5(e)), further indicating that the battery using O-Pd-Fe@NC/C possesses great discharge performance.

Further, in Fig. 5(f), the operation durability of the Zn-air battery with O-Pd-Fe@NC/C was investigated (10 min for discharge and 10 min for charge). For O-Pd-Fe@NC/C electrode, nearly no virtual loss can be observed even after cycling for 160 h. By contrast, the Pt/C electrode exhibits a large charge and discharge difference value. The cycling performance test demonstrates the superior stability of O-Pd-Fe@NC/C, which is due to the protective effect of N-doped carbon layer, ordered structure of Pd-Fe nanoparticles and the interface confinement interaction effect between them. As an illustration, in Fig. 5(g), two series-connected O-Pd-Fe@NC/C-based Zn-air batteries can power a LED panel (2.5–3 V) for a long time.

3 Conclusion

To summarize, we demonstrated an effective strategy to synthesize N-doped carbon layer encapsulated Pd-Fe ordered intermetallic nanoparticles as highly active and durable electrocatalysts toward ORR in both acid and alkaline medium. The *in situ* formed N-doped carbon shell can effectively prevent Pd-Fe intermetallic nanoparticles from agglomeration or coalescence. In addition, the N-doped carbon shell can also restrain the Pd-Fe ordered intermetallic nanoparticles from detachment and aggregation during the electrocatalysis. The enhanced ORR performance of O-Pd-Fe@NC/C observed is due to the strong anchoring effect of the N-doped carbon shell, the Pd-Fe nanoparticles with highly ordered atomic arrangement and the interface confinement effect between them. The excellent activity, durability, and anti-poisoning capacity of

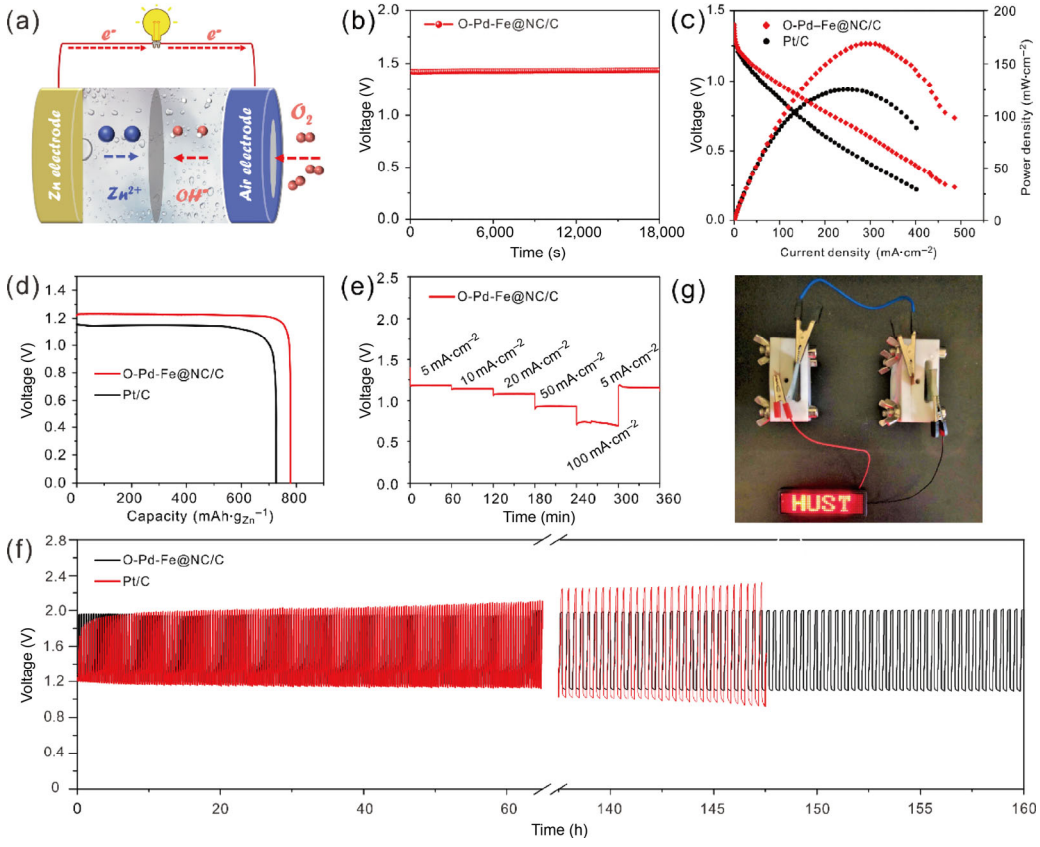

Figure 5 (a) Schematic diagram of the homemade Zn-air battery. (b) Long-time open circle potential test. (c) LSV and corresponding power density curves of Zn-air battery with the catalysts. (d) Discharge curves tested at current density of 5 mA·cm^{-2}. (e) Rate capacity test under different discharge current density. (f) Galvanostatic discharge and charge curves test at 5 mA·cm^{-2}. (g) Photography of LED panel (2.5–3 V) powered by two series-connected homemade Zn-air batteries based on O-Pd-Fe@NC/C catalysts.

O-Pd-Fe@NC/C may make it possible to replace Pt as a highly active and cost-effective electrocatalyst for practical application in fuel cells.

Acknowledgements

This work was supported by the National Natural Science Foundation of China (No. 91963109) and the Fundamental Research Funds for the Central Universities (No. 2172019kfyRCPY100). The authors thank the Analytical and Testing Center of HUST for allowing the use of its help and facilities for XRD and XPS. This research used resources of the UC IMRI facilities and the Center for Functional Nanomaterials, which is a U.S. DOE Office of Science Facility, at Brookhaven National Laboratory under Contract No. DE-SC0012704.

Electronic Supplementary Material: Supplementary material (detailed synthesis of O-Pd-Fe@NC/C and contrast materials, test parameter about the electrochemical performance and Zn-air battery, TEM of O-Pd-Fe@NC/C before and after durability test, TG analysis result, CV curves before and after 10,000 cycles in acid and base medium, *K-L* plots, anti-poisoning capability test and comparison of electrochemical performance of O-Pd-Fe@NC/C with catalysts previously reported) is available in the online version of this article at https://doi.org/10.1007/s12274-020-2856-z.

References

[1] Wang, D. L.; Xin, H. L.; Hovden, R.; Wang, H. S.; Yu, Y. C.; Muller, D. A.; DiSalvo, F. J.; Abruña, H. D. Structurally ordered intermetallic platinum–cobalt core–shell nanoparticles with enhanced activity and stability as oxygen reduction electrocatalysts. *Nat. Mater*. **2012**, *12*, 81–87.

[2] Gu, Y.; Liu, Y. F.; Cao, X. T. Evolving strategies for tumor immunotherapy: Enhancing the enhancer and suppressing the suppressor. *Nat. Sci. Rev*. **2017**, *4*, 161–163.

[3] Zhu, C. Z.; Dong, S. J. Recent progress in graphene-based nanomaterials as advanced electrocatalysts towards oxygen reduction reaction. *Nanoscale* **2013**, *5*, 1753–1767.

[4] Wang, X.; Wang, J.; Wang, D. L.; Dou, S.; Ma, Z. L.; Wu, J. H.; Tao, L.; Shen, A. L.; Ouyang, C. B.; Liu, Q. H. et al. One-pot synthesis of nitrogen and sulfur co-doped graphene as efficient metal-free electrocatalysts for the oxygen reduction reaction. *Chem. Commun*. **2014**, *50*, 4839–4842.

[5] Xiao, W. P.; Zhu, J.; Han, L. L.; Liu, S. F.; Wang, J.; Wu, Z. X.; Lei, W.; Xuan, C. J.; Xin, H. L.; Wang, D. L. Pt skin on Pd-Co-Zn/C ternary nanoparticles with enhanced Pt efficiency toward ORR. *Nanoscale* **2016**, *8*, 14793–14802.

[6] Lv, H. F.; Peng, T.; Wu, P.; Pan, M.; Mu, S. C. Nano-boron carbide supported platinum catalysts with much enhanced methanol oxidation activity and CO tolerance. *J. Mater. Chem*. **2012**, *22*, 9155–9160.

[7] He, D. P.; Tang, H. L.; Kou, Z. K.; Pan, M.; Sun, X. L.; Zhang, J. J.; Mu, S. C. Engineered graphene materials: Synthesis and applications for polymer electrolyte membrane fuel cells. *Adv. Mater*. **2017**, *29*, 1601741.

[8] Yin, S B.; Cai, M.; Wang, C. X.; Shen, P. K. Tungsten carbide promoted Pd–Fe as alcohol-tolerant electrocatalysts for oxygen reduction reactions. *Energy Environ. Sci*. **2011**, *4*, 558–563.

[9] Wang, G. W.; Guan, J. X.; Xiao, L.; Huang, B.; Wu, N.; Lu, J. T.; Zhuang, L. Pd skin on AuCu intermetallic nanoparticles: A highly active electrocatalyst for oxygen reduction reaction in alkaline media. *Nano Energy* **2016**, *29*, 268–274.

[10] Zhang, L.; Lee, K.; Zhang, J. J. The effect of heat treatment on nanoparticle size and ORR activity for carbon-supported Pd–Co

alloy electrocatalysts. *Electrochim. Acta* **2007**, *52*, 3088–3094.
[11] Luo, L. X.; Zhu, F. J.; Tian, R. X.; Li, L.; Shen, S. Y.; Yan, X. H.; Zhang, J. L. Composition-graded Pd_xNi_{1-x} nanospheres with Pt monolayer shells as high-performance electrocatalysts for oxygen reduction reaction. *ACS Catal*. **2017**, *7*, 5420–5430.
[12] Lim, B.; Jiang, M. J.; Camargo, P. H. C.; Cho, E. C.; Tao, J.; Lu, X. M.; Zhu, Y. M.; Xia, Y. N. Pd-Pt bimetallic nanodendrites with high activity for oxygen reduction. *Science* **2009**, *324*, 1302–1305.
[13] Gao, Q.; Ju, Y. M.; An, D.; Gao, M. R.; Cui, C. H.; Liu, J. W.; Cong, H. P.; Yu, S. H. Shape-controlled synthesis of monodisperse PdCu nanocubes and their electrocatalytic properties. *ChemSusChem* **2013**, *6*, 1878–1882.
[14] Zhang, L.; Hou, F.; Tan, Y. W. Shape-tailoring of CuPd nanocrystals for enhancement of electro-catalytic activity in oxygen reduction reaction. *Chem. Commun.* **2012**, *48*, 7152–7154.
[15] Liu, Z. Y.; Fu, G. T.; Li, J. H.; Liu, Z. Q.; Xu, L.; Sun, D. M.; Tang, Y. W. Facile synthesis based on novel carbon-supported cyanogel of structurally ordered Pd_3Fe/C as electrocatalyst for formic acid oxidation. *Nano Res.* **2018**, *11*, 4686–4696.
[16] Zhang, B. T.; Fu, G. T.; Li, Y. T.; Liang, L. C.; Grundish, N. S.; Tang, Y. W.; Goodenough, J. B.; Cui, Z. M. General strategy for synthesis of ordered Pt_3M intermetallics with ultrasmall particle size. *Angew. Chem., Int. Ed*. **2020**, *59*, 7857–7863.
[17] Xiao, W. P.; Cordeiro, M. A. L.; Gao, G. Y.; Zheng, A. M.; Wang, J.; Lei, W.; Gong, M. X.; Lin, R. Q.; Stavitski, E.; Xin, H. L. et al. Atomic rearrangement from disordered to ordered Pd-Fe nanocatalysts with trace amount of Pt decoration for efficient electrocatalysis. *Nano Energy* **2018**, *50*, 70–78.
[18] Zou, L. L.; Fan, J.; Zhou, Y.; Wang, C. M.; Li, J.; Zou, Z. Q.; Yang, H. Conversion of PtNi alloy from disordered to ordered for enhanced activity and durability in methanol-tolerant oxygen reduction reactions. *Nano Res*. **2015**, *8*, 2777–2788.
[19] Maiti, K.; Balamurugan, J.; Peera, S. G.; Kim, N. H.; Lee, J. H. Highly active and durable core-shell fct-PdFe@Pd nanoparticles encapsulated NG as an efficient catalyst for oxygen reduction reaction. *ACS Appl. Mater Interfaces* **2018**, *10*, 18734–18745.
[20] Galeano, C.; Meier, J. C.; Peinecke, V.; Bongard, H.; Katsounaros, I.; Topalov, A. A.; Lu, A. H.; Mayrhofer, K. J. J.; Schüth, F. Toward highly stable electrocatalysts via nanoparticle pore confinement. *J. Am. Chem. Soc*. **2012**, *134*, 20457–20465.
[21] Chen, H.; Wang, D.; Yu, Y. C.; Newton, K. A.; Muller, D. A.; Abruña, H.; DiSalvo, F. J. A surfactant-free strategy for synthesizing and processing intermetallic platinum-based nanoparticle catalysts. *J. Am. Chem. Soc*. **2012**, *134*, 18453–18459.
[22] Cheng, N. C.; Banis, M. N.; Liu, J.; Riese, A.; Li, X.; Li, R. Y.; Ye, S. Y.; Knights, S.; Sun, X. L. Extremely stable platinum nanoparticles encapsulated in a zirconia nanocage by area-selective atomic layer deposition for the oxygen reduction reaction. *Adv. Mater.* **2015**, *27*, 277–281.
[23] An, L.; Jiang, N.; Li, B.; Hua, S. X.; Fu, Y. T.; Liu, J. X.; Hao, W.; Xia, D. G.; Sun, Z. C. A highly active and durable iron/cobalt alloy catalyst encapsulated in N-doped graphitic carbon nanotubes for oxygen reduction reaction by a nanofibrous dicyandiamide template. *J. Mater. Chem. A* **2018**, *6*, 5962–5970.
[24] Choi, C. H.; Lee, S. Y.; Park, S. H.; Woo, S. I. Highly active N-doped-CNTs grafted on Fe/C prepared by pyrolysis of dicyandiamide on Fe_2O_3/C for electrochemical oxygen reduction reaction. *Appl. Catal. B Environ.* **2011**, *103*, 362–368.
[25] Li, Q.; Xu, D.; Guo, J. N.; Ou, X.; Yan, F. Protonated g-C_3N_4@polypyrrole derived N-doped porous carbon for supercapacitors and oxygen electrocatalysis. *Carbon* **2017**, *124*, 599–610.
[26] Wang, Y.; Wang, L.; Tong, M. M.; Zhao, X. J.; Gao, Y. T.; Fu, H. G. Co-VN encapsulated in bamboo-like N-doped carbon nanotubes for ultrahigh-stability of oxygen reduction reaction. *Nanoscale* **2018**, *10*, 4311–4319.
[27] Su, Y. H.; Jiang, H. L.; Zhu, Y. H.; Yang, X. L.; Shen, J. H.; Zou, W. J.; Chen, J. D.; Li, C. Z. Enriched graphitic N-doped carbon-supported Fe_3O_4 nanoparticles as efficient electrocatalysts for oxygen reduction reaction. *J. Mater. Chem. A* **2014**, *2*, 7281–7287.
[28] Guo, L.; Jiang, W. J.; Zhang, Y.; Hu, J. S.; Wei, Z. D.; Wan, L. J. Embedding Pt nanocrystals in N-doped porous carbon/carbon nanotubes toward highly stable electrocatalysts for the oxygen reduction reaction. *ACS Catal.* **2015**, *5*, 2903–2909.
[29] Arrigo, R.; Schuster, M. E.; Xie, Z. L.; Yi, Y. M.; Wowsnick, G.; Sun, L. L.; Hermann, K. E.; Friedrich, M.; Kast, P.; Hävecker, M. et al. Nature of the N–Pd interaction in nitrogen-doped carbon nanotube catalysts. *ACS Catal*. **2015**, *5*, 2740–2753.
[30] Perazzolo, V.; Grądzka, E.; Durante, C.; Pilot, R.; Vicentini, N.; Rizzi, G. A.; Granozzi, G.; Gennaro, A. Chemical and electrochemical stability of nitrogen and sulphur doped mesoporous carbons. *Electrochim. Acta* **2016**, *197*, 251–262.
[31] Hu, J.; Kuttiyiel, K. A.; Sasaki, K.; Su, D.; Yang, T. H.; Park, G. G.; Zhang, C. X.; Chen, G. Y.; Adzic, R. Pt monolayer shell on nitrided alloy core—a path to highly stable oxygen reduction catalyst. *Catalysts* **2015**, *5*, 1321–1332.
[32] Xiong, Y.; Yang, Y.; DiSalvo, F. J.; Abruña, H. D. Pt-decorated composition-tunable Pd-Fe@Pd/C core-shell nanoparticles with enhanced electrocatalytic activity toward the oxygen reduction reaction. *J. Am. Chem. Soc.* **2018**, *140*, 7248–7255.
[33] Liu, R. L.; Wu, D. Q.; Feng, X. L.; Müllen, K. Nitrogen-doped ordered mesoporous graphitic arrays with high electrocatalytic activity for oxygen reduction. *Angew. Chem., Int. Ed.* **2010**, *49*, 2565–2569.
[34] He, C. Y.; Shen, P. K. Pt loaded on truncated hexagonal pyramid WC/graphene for oxygen reduction reaction. *Nano Energy* **2014**, *8*, 52–61.
[35] Najam, T.; Shah, S. S. A.; Ding, W.; Jiang, J. X.; Jia, L.; Yao, W.; Li, L.; Wei, Z. D. An efficient anti-poisoning catalyst against SO_x, NO_x, and PO_x: P, N-doped carbon for oxygen reduction in acidic media. *Angew. Chem., Int. Ed*. **2018**, *57*, 15101–15106.
[36] Wen, Z.; Liu, J.; Li, J. Core/shell Pt/C nanoparticles embedded in mesoporous carbon as a methanol-tolerant cathode catalyst in direct methanol fuel cells. *Adv. Mater.* **2008**, *20*, 743–747.
[37] Choi, B.; Nam, W. H.; Chung, D. Y.; Park, I. S.; Yoo, S. J.; Song, J. C.; Sung, Y. E. Enhanced methanol tolerance of highly Pd rich Pd-Pt cathode electrocatalysts in direct methanol fuel cells. *Electrochim. Acta* **2015**, *164*, 235–242.
[38] Wang, J.; Wu, Z. X.; Han, L. L.; Liu, Y. Y.; Guo, J. P.; Xin, H. L.; Wang, D. L. Rational design of three-dimensional nitrogen and phosphorus co-doped graphene nanoribbons/CNTs composite for the oxygen reduction. *Chin. Chem. Lett*. **2016**, *27*, 597–601.
[39] Hu, L. B.; Yu, F.; Yuan, H. F.; Wang, G.; Liu, M. C.; Wang, L. N.; Xue, X. Y.; Peng, B. H.; Tian, Z. Q.; Dai, B. Improved oxygen reduction reaction via a partially oxidized Co-CoO catalyst on N-doped carbon synthesized by a facile sand-bath method. *Chin. Chem. Lett*. **2019**, *30*, 624–629.